Porphyrin Binding to Gun4 protein, Facilitated by a Flexible Loop, Controls Metabolite Flow through the Chlorophyll Biosynthetic Pathway

Jana Kopečná[1,$], Israel Cabeza de Vaca[3,$], Nathan B. P. Adams[4], Paul A. Davison[4], Amanda A. Brindley[4], C. Neil Hunter[4], Victor Guallar[3,5], Roman Sobotka[1,2]

[1]Institute of Microbiology, Academy of Sciences, Opatovický mlýn, 37981 Třeboň, Czech Republic

[2]Faculty of Science, University of South Bohemia, Branišovská 31, 370 05 České Budějovice, Czech Republic

[3]Joint BSC-CRG-IRB Research Program in Computational Biology, Barcelona Supercomputing Center, c/Jordi Girona 29, 08034 Barcelona, Spain.

[4]Department of Molecular Biology and Biotechnology, University of Sheffield, Sheffield, S10 2TN, UK

[5]Institució Catalana de Recerca i Estudis Avançats, Passeig Lluís Companys 23, 08010 Barcelona, Spain

*Running title**:** Role of porphyrin-binding by Gun4 protein

To whom correspondence should be addressed: Roman Sobotka, Institute of Microbiology, Opatovický mlýn, 379 81 Třeboň, Czech Republic. Tel ++420-384-340491; Fax ++420-384-340415; Email sobotka@alga.cz. Victor Guallar, Joint BSC-CRG-IRB Research Program in Computational Biology, Barcelona Supercomputing Center, c/Jordi Girona 29, 08034 Barcelona, Spain. Tel +34(93)4137727; Email victor.guallar@bsc.es.

[$] These authors equally contributed to this work.

Keywords: chlorophyll biosynthesis, *Synechocystis* 6803, Gun4, porphyrins, cyanobacteria, Mg-protoporphyrin IX

Background: The Gun4 protein stimulates activity of Mg-chelatase and it is important for chlorophyll biosynthesis.
Results: Mechanism of porphyrin-binding by Gun4 was proposed and a Gun4 mutant characterized in detail.
Conclusion: Gun4 controls substrate-channeling into chlorophyll biosynthesis.
Significance: For the first time *in silico*, *in vitro* and *in vivo* data were integrated to explain the function of Gun4 protein.

ABSTRACT

In oxygenic phototrophs, chlorophylls, hemes and bilins are synthesized by a common branched pathway. Given the phototoxic nature of tetrapyrroles, this pathway must be tightly regulated and an important regulatory role is attributed to Mg-chelatase enzyme at the branching between the heme and chlorophyll pathway. Gun4 is a porphyrin-binding protein known to stimulate *in vitro* the Mg-chelatase activity but how the Gun4-porphyrin complex acts in the cell was unknown. To address this issue we first performed simulations to determine the porphyrin-docking mechanism to the cyanobacterial Gun4 structure. After correcting crystallographic loop contacts, we determined the binding site for Mg-protoporphyrin IX. It revealed that the orientation of α6/α7 loop is critical for the binding and the magnesium ion held within the porphyrin is coordinated by Asn211 residue. We also identified the basis for stronger binding in the Gun4-1 variant and for weaker binding in the W192A mutant. The W192A-Gun4 was further characterized in Mg-chelatase assay showing that tight porphyrin-binding in Gun4 facilitates its interaction with the Mg-chelatase ChlH subunit. Finally, we introduced the W192A mutation into *Synechocystis* 6803 cells and show that the Gun4-porphyrin complex is important for the accumulation of ChlH and for channeling metabolites into the chlorophyll biosynthetic pathway.

Tetrapyrrole biosynthesis ranks amongst the most fundamental pathways in living systems, leading to production of heme, siroheme and vitamin B12. Synthesis of heme is conserved among all three domains of life, starting with synthesis of δ-aminolevulinic acid (ALA), which is converted through several enzymatic steps into protoporphyrin IX (P_{IX}) - an empty porphyrin ring. P_{IX} is a substrate for ferrochelatase, which catalyzes the insertion of iron to produce heme.

The tetrapyrrole biosynthetic pathway is more complex in photosynthetic organisms since, apart from heme, they usually require large quantities of other tetrapyrrole end-products. (Bacterio)chlorophylls are critical cofactors of the photosynthetic apparatus and cyanobacteria and red algae also produce large amounts of linear phycobilins serving for light capture in phycobilisomes. The synthesis of (bacterio)chlorophylls, hemes, and bilins shares the same pathway up until P_{IX}, where the ferrochelatase competes for the same substrate with magnesium chelatase (MgCh). Insertion of Mg^{2+} by MgCh leads to Mg-protoporphyrin IX (MgP), the first intermediate on the (bacterio)chlorophyll branch. This step is followed by methylation of MgP by MgP methyltransferase enzyme (ChlM).

Tetrapyrroles are phototoxic, so their biosynthetic pathway must be tightly regulated to prevent accumulation of intermediates. However, there are special features of this pathway in organisms performing oxygenic photosynthesis (cyanobacterial, algae and plants) that cause its regulation to be particularly important and complex. These organisms produce chlorophyll (Chl) and heme under light and in the presence of oxygen, which is a dangerous environment for dealing with high concentration of tetrapyrroles (1,2). Moreover, the relative levels of heme and Chl are quite different and the rate of their formation depends on actual growth conditions (3,4). Photosynthetic cells must control the total flow through the tetrapyrrole pathway while precisely distributing P_{IX} into heme and Chl

branches. There is likely a complex regulatory network securing the synthesis of tetrapyrrole end-products in requested amounts while keeping the intermediate concentration extremely low; reviewed in (5,6).

It is accepted that both ferrochelatase and MgCh play an important regulatory role in allocation of metabolites into the heme/Chl branches (6-9). Its mechanism, however, is far from clear. Ferrochelatase is a single-protein enzyme but MgCh requires three subunits (ChlH, ChlI, ChlD) for activity. In bacteriochlorophyll-producing bacteria these three subunits are sufficient for a highly active MgCh enzyme when assayed *in vitro* (10). In contrast, MgCh from cyanobacteria, algae and plants requires a protein called Gun4 that strongly enhances MgCh activity *in vitro* (11-13), and very likely also *in vivo* (14,15).

Gun4 was shown to bind various porphyrins, exhibiting the highest affinity to MgP, the product of MgCh enzyme, and a weaker affinity to P_{IX} (13,16). There is evidence that Gun4 physically interacts with ChlH (11,14,17), which is the porphyrin-binding MgCh subunit that presumably also contains the active site for chelation (18). Available *in vitro* kinetic data imply that Gun4 stimulates MgCh by substantially reducing the P_{IX} and Mg^{2+} concentrations required for catalysis (12). Inactivation of the *gun4* gene perturbs Chl biosynthesis and accumulation of Chl-binding proteins in cyanobacteria (14), green algae (15) as well as in plants (11,19). However, phenotypes of available Gun4 mutants are difficult to explain simply by a defect in MgCh activity and the *in vivo* activities of Gun4 appears to be complex (15,19,20).

Although it is widely accepted that the role of Gun4 depends on tight porphyrin binding (20,21), there is no conclusive model of how is the Gun4-porphyrin complex is implicated in controlling of tetrapyrrole biosynthesis. Here, we employed *in silico* modeling, which allows us to identify the MgP-binding pocket and provides atomic description of the MgP-binding mechanism for cyanobacterial Gun4. Having a detailed view on interactions between Gun4 and MgP, we replaced Trp192 reside to obtain a Gun4 variant (W192A) with significantly weakened affinity to porphyrins. The W192A mutation was explored *in vitro* in a MgCh assay and *in vivo* in the cyanobacterium *Synechocystis* 6803 (hereafter *Syn*). These experiments revealed that the weaker affinity of W192A-Gun4 to porphyrins compromised the formation of Gun4-ChlH complex. As the *Syn gun4-W192A* strain was deficient in Chl precursors and exhibits a defect in accumulation of ChlH and ChlM the porphyrin-driven interaction between Gun4-ChlH appears to be crucial for the formation and mainteinanace of active MgCh enzyme.

EXPERIMENTAL PROCEDURES

Molecular dynamics

Simulations were performed with the AMBER11 molecular modeling suit (22). All systems were first prepared at pH 7.7 using the Protein Preparation Wizard from Schrodinger (23). The parm99 force field was used to define the parameters of the proteins in combination with a truncated octahedron water box containing ~24000 TIP3P water molecules. Na^+ and Cl^- ions were added to neutralize and reach an ionic strength of 0.15 M. After standard equilibration, we performed 200 ns of molecular dynamics at constant pressure and temperature (NPT ensemble) using the Berendsen barostat and thermostat. RMSF analysis was performed using python PRODY library and cross-correlations maps were computed using ptraj tool from the Ambertools 13 package.

Loop prediction

The Prime loop prediction tool (Prime, version 3.8, Schrödinger, LLC, New York, USA) was used to model conformations of α2/α3 and α6/α7 in the Gun4 core domain. Due to the size of the loops, we used the extended loop prediction options. Side chains with less than 7.5 Å of separation were also refined and the 10 lowest energy structures were minimized. The crystal symmetry option was used to predict the effect of crystal contacts. Dielectric constants

were 1 and 80 for the (solvent exposed) internal and external environments, respectively.

Simulation of the porphyrin binding to Gun4 by PELE

PELE (Protein Energy Landscape Exploration) (PELE), a Monte Carlo algorithm developed specifically to explore protein ligand interactions (24), was used to model porphyrin binding. In PELE each Monte Carlo step is comprised by two main parts: perturbation and relaxation. Perturbation consists of a random translation and rotation of the ligand plus an anisotropic network model (ANM) procedure to model backbone fluctuations. Relaxation involves optimization of the side chains local to the ligand and a global minimization. Then, the step is rejected or accepted using a metropolis criterion to generate a realistic distribution of the configurations generated.

Entrance simulations initially placed the ligand in the bulk solvent, outside of the binding site. Using the spawning algorithms in PELE, the ligand was then asked to enter into the active site. This algorithm constrains the ligand random search in a sphere around 18 Å from a given (chosen) point. If the ligand escapes this sphere, it will be placed in the closest conformation to the reference given point found by any explorer (trajectory). The Alpha carbon in Phe160 was used as the spawning center (representative of an active site position).

PELE was able to find binding poses in ~24 hours using 48 trajectories (with 1 trajectory per computing core), using random translations and rotations in the 1-7Å and 0-90˚ ranges, respectively. Once the ligand reached the active site, a local refinement explorations used a smaller spawning sphere, 10 Å, and a smaller translation of 0.5 Å to better explore the binding energy profile in the bound region. 240 trajectories times 24 hours were used in the refining process for a total of ~50,000 accepted steps.

Construction of the Syn *mutant strains and the growth conditions*

In order to prepar*e Syn* Δ*gun4*, we made a linear PCR construct by method of (25) containing the zeocin resistance cassette fused with *gun4* flanking sequences (~300 bp) to allow homologous recombination. After transformation into WT cells and segregation, the zeocin cassette replaced almost the entire *gun4* gene (bp 119 – 694).

For the construction of the *Gun4W192A* strain we cloned the chromosomal fragment containing the *gun4* gene and 300-bp DNA upstream and downstream flanking regions into pUC18 vector (Life Technologies) between *Eco*RI and *BamH*I restriction sites. The W192A mutation was inserted into the cloned *gun4* gene using the QuikChange II Site-Directed Mutagenesis Kit (Agilent Technologies). The pUC18-*Gun4W192A* plasmid was transformed into the above-described *Syn* Δ*gun4* strain and photoautotrophic transformants were selected on BG11 agar plates at 28°C and 30 μmol photons m^{-2} s^{-1}. *Syn* cells were grown in liquid culture in 250 ml Erlenmeyer flasks on a rotary shaker at 28°C and bubbled with air.

Absorption spectra, determination of Chl content and quantification of Chl precursors

Absorption spectra of whole cells were measured at room temperature using a Shimadzu UV-3000 spectrophotometer (Kyoto, Japan). Chl was extracted from cell pellets (1 mL, OD_{750} ~ 0.4) with 100% ($^{V}/_{V}$) methanol, and its concentration was measured spectrophotometrically according to (26). For the quantitative determination of Chl precursors in *Syn* cells, 2 mL of culture at OD_{750} ~ 0.4 were quickly harvested and the extracted pigments analyzed essentially as described in (27).

Electrophoresis and immunoblotting

To analyze protein levels, *Syn* cells in an exponential growth phase (OD_{750} ~ 0.4) were harvested by centrifugation, washed, resuspended in the buffer containing 25 mM

Hepes/NaOH, pH 7.4, 5 mM $CaCl_2$, 10 mM $MgCl_2$, and 20% $^{w}/_{V}$ glycerol, and broken using glass beads. Cell extracts were further denatured in 2 % SDS and 1 % DTT for 30 min at room temperature and separated in a 10 % polyacrylamide gel using a mini BioRad system. For Western blotting, proteins were transferred onto a PVDF membrane (Sigma, Germany), probed with specific primary antibodies followed by the secondary antibody conjugated to horseradish peroxidase (Sigma, Germany). The primary antibody raised against recombinant *Syn* Gun4 was kindly provided by Prof. Annegret Wilde (Universität Freiburg, Germany).

Circular dichroism spectra, tryptophan quenching, and in vitro MgCh enzyme assays

To obtain recombinant Gun4 and W192A proteins, the *Syn gun4* gene was cloned into the pET14(b) plasmid and purified as for the *T.el* protein as reported previously (28). The W192A mutation was introduced into the pET14(b):*gun4* plasmid by the same procedure used for construction of the *Syn gun4W192A* strain (see above). Recombinant subunits of *Syn* MgCh were expressed and purified as described in (29).

CD spectra were recorded using a JASCO-810 spectometer (JASCO, Great Dunmow, UK). Protein was dissolved in water to a concentration of 1 mg ml^{-1}, and analysed in a cuvette with a 0.2 cm path length. Spectra were recorded stepwise, from 250 – 190 nm in 1 nm increments, 4 seconds/nm.

Porphyrin-binding studies were carried out on a Yobin Yvon Fluoromax 3 spectofluorometer fitted with a temperature-controlled cuvette holder. The samples consisted of 1 µM protein in 50 mM MOPS/KOH, 11 mM KCl, 1 mM DTT, 0.3 M glycerol, pH 7.7 at 34 °C. Titrations were performed by addition of porphyrin and incubated for 2 minutes before recording of fluorescence (λex = 280 ± 4.5 nm, λem = 350 ± 18 nM). Changes in volume were < 5 %, and were taken into account in calculating dissociation constants by using the titration mode in DynaFit 4 (Biokin Ltd.).

Functional MgCh enzyme assays were performed essentially as described previously (17). Calibration curves using known standard concentrations of MgD were created for each concentration of Gun4 analyzed. Plots of MgCh steady state activity with respect to Gun4 concentration were fitted using Igor Pro (Wavemetrics Inc) to provide apparent constants for the formation of the MgCh.Gun4 complex (K_{app}). At high (8 µM) D_{IX} concentrations, activity of MgCh is inhibited when Gun4 reaches high concentrations. These data were fitted to equation 1, which allows for this observed inhibition by calculating an apparent inhibition constant (K^{i}_{app}). At low concentrations of D_{IX} (0.8 µM), no inhibition is observed in the Gun4 concentration range observed, therefore equation 2 was used to obtain estimates of complex formation. In equations 1 and 2, v_{ss} is the observed rate of MgCh, v_{ss} is the rate of MgCh in absence of Gun4 and V_{max} is the theoretical maximum rate.

$$v_{ss} = c + \left(\frac{V_{max}}{1 + \frac{K_{app}}{[Gun4]} + \frac{[Gun4]}{K^{i}_{app}}} \right) \quad \text{Equation 1}$$

$$v_{ss} = c + \left(\frac{V_{max}}{1 + \frac{K_{app}}{[Gun4]}} \right) \quad \text{Equation 2}$$

RESULTS

Comparison of available crystal structures of Gun4 proteins and the prediction of loops

In order to study the role of porphyrin binding by Gun4 protein, we performed *in silico* modeling, where recent developments (mainly motivated by the pharmacological industry) have allowed an accurate all-atom description of the ligand binding mechanism for complex systems such as Gun4 (30-32). First, we inspected the three available Gun4 crystal structures, all in the porphyrin-free form, deposited in the Protein Data Bank when this project commenced: the *Syn* Gun4 protein (13), and the Gun4 and so

called Gun4-1 mutant (L105F) from another cyanobacterium *Thermosynechococcus elongatus* (hereafter *T.el*; 12). We note that two more structures have been reported since (33,34). As previously reported (12), *T.el* Gun4 and L105F structures are practically identical except for the L105F change. *Syn* and *T.el* WT structures, however, show large differences in orientation of α2/α3 and α6/α7 loops (Fig. 1), part of the highly conserved Gun4 core domain (13). Based on an extensive analysis of site-directed *Syn* Gun4 mutant proteins and NMR chemical shift measurements, this core domain was proposed as the porphyrin binding pocket (Fig. 1; 13). However, it should be noted that docking of MgP into the binding pocket as proposed by (13) is not possible for *Syn* Gun4. The tight packing derived from the above loop orientations introduces severe steric clashes returning no bound poses from standard docking approaches.

Interestingly, while the α2/α3 loop has high atomic crystal β-factors, the α6/α7 one presents quite low scores, indicating its rigidity (not common in such a large loop) or constrained nature. Indeed, inspection of the X-ray symmetric unit indicated critical crystallographic contacts capable of defining (constraining) the α6/α7 loop position. The number of interactions in this region is larger in *Syn* Gun4 and also their nature (salt bridge) is stronger. In particular, in the *Syn* Gun4 we find Trp192-Glu7, Arg191-Glu49 and Thr190-Glu49 contacts, whereas in the *T.el* structure we only observe the Lys192-His69 one. The conformational mobility of the α6/α7 loop appears to drive a change in the mobile α2/α3 adjacent loop, which further restricts the porphyrin access into the putative binding pocket (Fig. 1).

To check if these contacts produce crystallographic artifacts in the loops, we performed loop prediction in presence and absence of crystal mates. In solution, where no crystal mates are included, the predicted α6/α7 loop for the *T.el* Gun4 is more closed, but still similar to the original structure with an overall open conformation. The predicted *Syn* Gun4 structure, however, drastically changes from the crystal structure (Fig. 1B), with an overall alpha carbon RMSD of 6.1 Å and an open structure similar to the one obtained from *T.el*. Additionally, the α2/α3 loop also significantly moved in the predicted *Syn* Gun4, further opening the cavity (Fig. 1C). We also noted that the conserved aromatic Trp192 residue, located at the α6/α7 loop, markedly turned and adopted a similar position to the homologous Tyr197 residue in *T.el* Gun4 (Fig. 1B). The Trp192/Tyr197 residue has been reported to be important for porphyrin binding (12) and therefore we selected a Trp192 mutant Gun4 for *in silico*, *in vitro* and *in vivo* analysis.

The Prime loop prediction software allows running simulations taking into account the crystallographic symmetry by adding neighboring units into the model. Assuming neighboring sidechains help to constrain loop structures, in such a case, one would expect to reproduce the crystal structure. This is actually what happens in Gun4, where simulations with crystal mates produce loops with a ~1-2 Å alpha carbon RMSD with respect to the crystallographically determined structures (hardly distinguishable from the experimental structures). Taken together, these results on both systems point to a strong bias in the loop conformation mediated by crystallographic contacts; thus, the conformation of functionally important loops in Gun4 cannot be assessed purely on the basis of crystallographic data, and study/correction with *in silico* methods (now a well-established practice; 35), is required. Importantly, this bias, originating from the structural data for *Syn* Gun4, produces a conformation with the loop restricting the access to the expected binding pocket. Thus, we adopt the corrected semi-open loop conformation, as modeled in solution by Prime, for the next round of simulations.

Molecular simulations of porphyrin binding into WT and mutant Syn Gun4 proteins

To map the porphyrin binding mechanism, we performed simulations where the ligand, starting in the bulk solvent, is asked to enter the binding site. We focused on the *Syn* Gun4 structure since

a detailed analysis of site-directed mutants has been already performed together with NMR measurements (13). In addition, *Syn* Gun4 mutants can be explored using both *in vitro* and *in vivo* systems. Figure 2 shows four different snapshots underlining the porphyrin docking mechanism into *Syn* Gun4 as observed in the PELE simulation (the entire migration movie can be seen in Suppl. movie 1). In panel A we show the initial structure where we placed the porphyrin ligand in the bulk solvent outside the Gun4 binding pocket. Panel B shows a recurrent pre-docking pose for the protein surface observed for both metal and non-metal porphyrins. In this pose, the porphyrin stacks onto the Arg113 side chain and forms hydrogen bonds with two glutamines (Gln126 and Gln128) present in the α2/α3 loop. From this pre-docking site, the porphyrin moves into the binding pocket forming an interesting axial coordination-like motif with Asn211 and Arg113; we named this site binding pocket-A (Fig. 2C, Fig. 3A). As shown below, this structure represents a steady-state in protein-ligand interaction energy From this pose, however, the porphyrin can migrate deeper into the binding pocket with less ligand exposure to solvent, and with porphyrin propionate groups anchored by interactions with Arg214 and Asn211; we named this site binding pocket-B (Fig. 2D, Fig. 3B).

To better characterize the porphyrin binding mode, we performed a refinement search where MgP, starting at pocket-A, is allowed to explore up to 10 Å distance (measured as the ligand center of mass displacement to the Asn211 side chain oxygen). Fig. 4A shows the protein-MgP interaction energies for the 50000 configurations sampled in this refinement procedure. We clearly observe the existence of two minima, which correspond to binding pockets A and B, with similar (~degenerate) interaction energies. We note that these interaction energies are derived from a classical force field not including any metal coordination component (beyond electrostatic attraction).

To distinguish which of these two minima might better represent the biological system, we compared interacting residues with previously reported studies of side-directed Gun4 mutants (12,13). Indeed, a number of residues which affect binding are involved in both positions (Fig. 3). However, a mutation in Asn211, which is placed in a coordination position with MgP in the less-deeper pocket-A (Fig. 3A) has been shown to exert significantly effect on the affinity of the MgP analog Mg-deuteroporphyrin IX (MgD) than for deuteroporphyrin IX (D_{IX}) (12). Additionally, the residue homologous to Trp192 in *T.el* (Tyr197), which participates directly in binding only in pocket-A (Fig. 3A), is required for high affinity porphyrin binding (12), see below. On the other hand, replacement of Ser221 has almost no effect on binding (13), which is not in agreement with the situation in pocket-B, where Ser221 forms a hydrogen bond to MgP (Fig. 3B). These are strong indications that the less-deep docking position-A is closer to the real binding pocket.

To further verify our model we studied the W192A mutant. This residue and Tyr197 are oriented differently in the original *Syn* and *T.el* structures (Fig. 1) but, after loop prediction and docking, Trp192 and Tyr197 are both exposed into the proposed binding pocket A (Fig. 1B, Fig. 3A). First, we compared recombinant *Syn* WT and Gun4-W192A proteins. Circular dichroism spectra showed that the WT and W192A Gun4 have very similar secondary and tertiary structures (Fig. 5). However, a difference in 200-210 nm region indicates a slightly more compact fold for the W192A protein. Indeed, the affinities of the mutated Gun4 for D_{IX} and MgD were 2 and 3 times weaker than the WT, respectively (Table I). Then we repeated the PELE local refinement search for W192A, observing that the mutant has slightly higher interaction energies and lower density of points at the bottom of the minima. To better quantify this, we binned all points in groups of 4 kcal/mol (Fig. 4B). By doing so, we can now appreciate more clearly the weaker (shift in) interaction energies for the W192A mutant. The direct role of Trp192 on porphyrin binding is evident from our detailed atomic simulations: inspecting the WT structures along the refinement trajectories, we observe the direct interaction between the Trp192 side chain

and the porphyrin group (Fig. 6 and Suppl. movie 2).

Dynamic simulations of T.el WT and L105F Gun4 proteins: cross-correlation maps

Gun4-1 mutation was originally identified in a chlorophyll-deficient Arabidopsis mutant with lesions of signaling between the chloroplast and nucleus (ref). The basis for the effect of the Leu → Phe (L105F in *T.el* Gun4) missense mutation has not been elucidated. Our model shows that while the *Syn* Trp192 residue is in direct contact with the bound porphyrin model, Leu105 in *T.el* Gun4 is located far away from the porphyrin binding site (Fig. 1). Moreover, WT and Gun4-1 *T.el* crystal structures do not show significant differences (12). Therefore, the mechanism by which the enigmatic Gun4-1 mutation confers a much tighter porphyrin binding (K_d for D_{IX} and MgD decreased 15-fold and 11-fold respectively; (12)) poses a real challenge. In order to address this issue, and seeking for possible dynamical effects, we employed molecular dynamics simulations.

We performed 200 ns molecular dynamics simulations of *T.el* Gun4 and Gun4-L105F and analyzed the dynamics with RMSF (root mean square fluctuation) and cross correlation maps. As seen in Figure 7A, replacement of Leu105 by Phe produces a significant change in the RMSF of several regions up to 1Å. The most important change concerning porphyrin-binding is the clear loss of mobility in the α6/α7 loop (residues 175-215) for the L105F mutant. The (residue movement) difference cross correlation map, shown in Figure 7B, allowed us to establish the mechanism for such a reduction in mobility. If we follow the position around Leu105, we clearly see two main correlated (red) groups (marked in Fig. 7B). As expected, several residues of helix 2 (110-125) in contact with Leu105, are correlated in their motion. More importantly, residues of the α6/α7 loop exhibit marked correlation with Leu105.

Effect of the W192A mutation on MgCh activity and Chl biosynthesis

In order to understand the physiological role of Gun4 in the cell we extended the mechanistic description arising from our binding model and performed kinetic and *in vivo* analyses on the W192A and WT Gun4 proteins. The ability of the W192A mutant to stimulate MgCh activity was assessed by titrating either *Syn* Gun4 WT or W192A recombinant protein into MgCh assays and monitoring the steady state rate. The more water-soluble porphyrin D_{IX} was used as a substrate instead of P_{IX}. Both Gun4 and W192A stimulated activity approximately 3-fold compared to MgCh activity alone. However, at high concentrations of D_{IX} substrate (8 μM) the K_{app} (the apparent binding constant for MgCh-Gun4 complex formation) suggests that the Gun4 WT has almost 3-fold tighter binding with MgCh compared to the W192A mutant. At low concentrations (0.8 μM D_{IX}) this effect was even more pronounced with a 4-fold difference in K_{app} between WT and W192A, and a 50 % decrease in V_{max} between WT and W192A (Table II). At 8 μM D_{IX} there is evidence of inhibition at high concentrations of Gun4 (Fig. 8, closed symbols).

Together, these data imply that the lowered affinity of Gun4 to porphyrin leads to a weaker interaction between the mutated Gun4 and the core MgCh complex, and this defect is emphasised at low substrate concentrations.

To monitor possible effects of the W192A mutation in *vivo*, we constructed a *Syn gun4-W192A* strain possessing the *gun4-W192A* allele instead of the original *gun4* gene. Mutated cells exhibited no difference in phycobilisome content but contained 20% less Chl under moderate light conditions (30 μE of photons) and 35% less Chl under saturating light (300 μE of photons; Fig. 9A). Under these conditions the cellular levels of mutated Gun4, ChlH and ChlM were comparable with WT (Fig. 9B) however, the mutant contained significantly more ChlI associated with membranes (Fig. 9B). In order to identify how the W192A mutation affects Chl biosynthesis, we analyzed pools of all

intermediates in the tetrapyrrole pathway from coproporphyrin(ogen) III (CoPP) to chlorophyllide. Detection was based on a separation by an HPLC system connected with two fluorescence detectors (Fig. 9C). Notably, even under moderate light intensity, the mutant exhibited significantly decreased levels of MgP, MgP methyl ester and both the monovinyl and divinyl forms of protochlorophyllide. However, the mutant did not accumulate P_{IX}, in fact, levels of CoPP and P_{IX} were rather lower in the mutant (Fig. 9C).

The result of the kinetic study of MgCh enzyme *in vitro* (Table II) indicated that the effect of the W192A mutation *in vivo* should be more pronounced when the level of MgCh substrate P_{IX} decreases. To mimic such situation we depleted pools of Chl precursors by incubating cells for 12 hours in a growth medium without nitrogen (Fig. 10A). After this treatment the only detectable Chl precursor is monovinyl-chlorophyllide that, however, originates from dephytilation of existing Chl and not from de novo synthesis (36). Chl biosynthesis was re-started by adding of $NaNO_3$ and after 2 hours a divinyl-protochlorophyllide peak became visible in WT chromatograms (Fig. 10B). In the *gun4-W192A* strain the Chl biosynthesis is much delayed; there is no detectable protochlorophyllide pool and the amount of MgP methyl ester is ~ 20% of that in the WT. Levels of CoPP and P_{IX} were however similar (Fig. 10B) in both strains, suggesting that either the flux through the whole pathway is down-regulated in the mutant and/or any excess of P_{IX} is metabolized by ferrochelatase. Levels of WT and mutated Gun4 changed just slightly during nitrogen starvation but the ChlI subunit and the ChlM enzyme were significantly reduced and the ChlH subunit almost completely disappeared in both strains (Fig. 9B). Interestingly, after adding nitrogen, both the ChlH and ChlM started to accumulate and this accumulation was apparently delayed in the mutant (Fig. 9B). We can therefore conclude that the Gun4-porphyrin complex is important for quick re-activation of Chl biosynthesis after a period of nutrient stress.

DISCUSSION

Mechanism of porphyrin binding into Gun4 protein

Gun4 is required for the synthesis of sufficient amounts of Chl in all groups of oxygenic phototrophs. It also appears that Gun4s from virtually all sources stimulate MgCh activity via an interaction with the ChlH subunit, and bind porphyrins, with the highest affinity to MgP (14,16,17). The essential role of porphyrin-binding for Gun4 function can be suggested from amino-acid alignments (13) as residues in the proposed MgP binding site (α6/α7 loop residues, Arg214, Asn211) are conserved through evolution from cyanobacteria to plants.

NMR data, crystal structures and site-directed mutagenesis suggested that the porphyrin binding region lies within the pocket formed at the intersection of the hydrophobic α6/α7 loop, the α2/α3 loop and by helices α2 and α7 (Fig. 1). However, the mechanism of the Gun4 – porphyrin interaction and how Gun4 discriminates between empty and metal-bound porphyrins remained unknown.

Our data imply that the orientation of the α6/α7 loop is critical for porphyrin binding. After removing the crystallographic artifacts, arising from protein-protein interactions in the crystal, the α6/α7 loop in both *Syn* and *T.el* Gun4 adopted a similar configuration, indicating that the shape of the loop is conserved (Fig. 1B,C). The observed flexibility of the α6/α7 loop and its possible conformational changes after porphyrin binding are consistent with changes in NMR-determined chemical shifts upon addition of D_{IX} (13).

An important finding of our simulation is the ability of Asn211 to co-ordinate MgP, which offers an explanation of the stronger affinity for MgP than P_{IX}, demonstrated experimentally (Table I). As described earlier we expect that the binding pocket-A, which includes co-ordination of MgP by Asn211 (Fig. 3A), is closer to the real pocket. Interestingly, the replacement of Trp192 by alanine had stronger effect on the binding of

MgD than to D_{IX} yielding a Gun4 with almost equal affinity for both these porphyrins (Table I). It is possible that the Trp192 is critical for the positioning of MgP in the proximity to Asn211. It would be interesting to employ PELE to compare binding energies for MgP and P_{IX} in WT and W192A mutant. However, the lack of accuracy when describing metal interactions by classical force fields does not allow a quantitative comparison between these two porphyrins.

While this paper was under review a *Syn* Gun4 structure with bound MgD has been deposited to the Protein Data Bank (33). In this structure the loop orientation is more opened than predicted by our modeling work and therefore the bound MgD is in a more planar orientation with respect to the α6/α7 loop and it lies closer to Helix 7. However, the main conclusions we derived from the simulations are valid: the α6/α7 loop residues are crucial for the formation of a relatively shallow binding pocket, MgP is coordinated by Asn211 and also the Trp192 residue interacts with MgD essentially as we proposed.

Asn211 is highly conserved and we speculate that the co-ordination is a universal feature of Gun4 proteins. On the other hand, there might be some variability in orientation of porphyrin propionates groups between cyanobacterial and plant Gun4s. According to (16) the homologue Arg214 residue in Arabidopsis Gun4 shows a defect in MgP binding, although it is not essential unlike in the *Syn* counterpart.

The Gun4-1 mutation was originally identified in Arabidopsis as the one of several *genome uncoupled* mutations causing modified plastid-to-nucleus signaling (37). The level of Gun4-1 protein in *Arabidopsis* is very low (11), however this mutation was characterized later using recombinant *T.el* and *Syn* Gun4-1 proteins that both exhibit an approximately ten-fold higher affinity for porphyrins than the WT Gun4 (12). Our results based on molecular dynamic simulations show a clear steric pathway connecting Leu105 with Helix 2 and the α6/α7 loop (Fig. 7), where the loss of mobility is effectively transmitted. Indeed, restricted flexibility of the Helix 2 and the α6/α7 loop can significantly affect the porphyrin binding supporting the critical role of these segments in our docking model (Fig. 2).

The role of Gun4 in regulation of tetrapyrrole biosynthesis

Although Gun4 proteins bind a broad spectrum of porphyrins including heme *b* or pheophorbide (16), MgP might be the crucial ligand *in vivo*, since there is evidence that only the binding of MgP (the product of MgCh) but not P_{IX} (MgCh substrate) enhances MgCh activity. This assumption is based on an *in vitro* analysis of *Syn* Gun4 proteins mutated at residues critical for binding D_{IX} but not for binding MgD and vice versa. Mutants of Gun4 where D_{IX} binding is abolished are still able to stimulate MgCh activity, whereas Gun4 mutants incapable of binding MgD completely failed to stimulate MgCh (13). These results suggest that Gun4 is implicated in release of the product (MgP) from ChlH. The fact that MgP is co-ordinated by the highly-conserved Asn211 indicates that the Gun4 has evolved to bind MgP (or to bind it better then P_{IX}) and connects the function of Gun4 with binding of this porphyrin. In the *in vitro* assay at limiting concentrations of D_{IX}, W192A-Gun4 is less effective in stimulating the MgCh enzyme due to the compromised interaction between Gun4 and the MgCh complex (Table II). It is not known when Gun4 binds to ChlH during the catalytic cycle of MgCh, but it appears that the high affinity of Gun4 to the MgP product facilitates a transient assembly of a Gun4-MgCh complex, stimulating MgCh activity. We expect that a similar defect also occurs *in vivo* in *Syn gun4-W192A* cells (see below).

The *in vivo* results obtained for various Gun4 mutants show complex changes in tetrapyrrole metabolism and it could be misleading to describe Gun4 simply as an enhancer of the MgCh enzyme. Overexpression of Gun4 in plants causes an aberrant accumulation of Chl, accompanied by elevated steady-state levels of

P_{IX} and MgP porphyrins (19). In the green alga *Chlamydomonas reinhardtii,* overexpression of Gun4 also increases Chl content per cell (38), while a *C. reinhardtii* strain possessing a low Gun4 content has reduced both Chl and P_{IX} levels (15,20). Only after the complete elimination of Gun4 cyanobacteria, algae and plants accumulate aberrant concentrations of P_{IX} (14,20,39).

To discuss the role of Gun4 in controlling Chl biosynthesis, one has to be careful in comparing data obtained from different organisms and under different growth conditions. However, the Gun4 mutations are generally more pronounced with increasing light intensity (14,19,38). The sensitivity of Gun4-less mutants to light and changes in ALA synthesizing capacity led to a hypothesis that Gun4 binds excessive porphyrins, which serves as a signal to down-regulate ALA formation (19,20). Although this model can explain reduced ALA synthesis in Gun4 or MgCh mutants (40), it is not consistent with the massive accumulation of P_{IX} in ferrochelatase mutants (8,41).

We propose an alternative model taking into account that Gun4 has been detected as a part of large membrane complexes (11). Under conditions when *Syn* cells reach maximal growth rate (saturating light, intensively air-bubbled culture) Gun4 and ChlH are localized almost exclusively in membrane fraction (Fig. 9B). Thus, the synthesis of MgP is quite certainly located in a membrane-associated complex where Gun4 is interacting with ChlH (21) and presumably also with the following enzyme ChlM (42). Although it has been reported that in plants the association of Gun4 with the membrane requires porphyrins (21), we detected Gun4 in membrane fraction even in cells lacking virtually all Chl intermediates except chlorophyllide (Fig. 9B). Also weaker affinity to porphyrins (W192A-Gun4) or a very low content of ChlH (nitrogen depletion) does not prevent Gun4 from associating with membranes and does not significantly alter the Gun4 level (Fig. 9B). This robustness contrasts with disappearance of ChlH during nitrogen depletion and its re-synthesis once nitrogen became available. As the affinity of Gun4 to porphyrins correlates with affinity of Gun4 to MgCh enzyme during catalysis (Table II) we propose that in the presence of P_{IX} or MgP the interaction of Gun4 with ChlH helps to stabilize a membrane-associated MgCh/ChlM complex. A Gun4-porphyrin complex can modulate disassembly and re-assembly of this enzymatic unit and thereby expose individual components to a post-translational control. It should be noted that in both cyanobacteria and plants, MgCh subunits are present even in the absence of Gun4 (14,19). Gun4 is not essential for the synthesis/stability of these proteins but it might be a critical component allowing cells to maintain optimal channeling of P_{IX} into the Chl metabolic branch. This role would be particularly important under fluctuating conditions requiring well-tuned de-activation and re-activation of MgCh and ChlM enzymes.

Consistent with this model, the Arabidopsis Gun4-less mutant is much more sensitive to a fluctuating light regime. Under continuous low light, the mutant can be partly complemented by supplementing with ALA (24). Interestingly, in Arabidopsis lacking Gun4, the level of ChlM is drastically reduced under fluctuating conditions, but it is restored by increasing the P_{IX} concentration by exogenous ALA (19).

According to available data it appears that there is cross-talk between the activity of MgCh-Gun4 complex and regulation of the metabolite flux through the whole tetrapyrrole pathway, keeping the P_{IX} pool small (19,20,40,43). As already discussed, other enzymes in the tetrapyrrole pathway, including ferrochelatase, could be a part of the identical membrane domain (5), it is therefore not difficult to imagine that the deactivation of MgCh allows ferrochelatase to attenuate ALA-formation *e.g.* via a heme-feedback loop (6). We observed that ferrochelatase is upregulated during nitrogen starvation (Fig. 9B). The presence of Gun4 in such a complex might be structurally important, which would explain why its complete elimination causes accumulation of P_{IX}. As already noted, a low level of Gun4 is sufficient for the balancing of P_{IX} pool (15).

In this work, we demonstrated that replacement of Gun4 by a variant with lower affinity to porphyrins reduced pools of intermediates in the Chl branch, but CoPP and P_{IX} levels are less affected. As expected from *in vitro* data the effect of this mutation is more pronounced once the mutated cells have to deal with fluctuations of metabolites in the tetrapyrrole pathway. The docking of MgP in Gun4 and the model of Gun4-based regulation described here can serve as a framework for future studies addressing the Gun4 function.

ACKNOWLEDGMENTS

This work was supported by project P501/12/G055 of the Czech Science Foundation, and by the National Programme of Sustainability I (LO1416) and by ERC 2009-Adg25027-PELE (to V.G). J.K. was supported by project Algain (EE2.3.30.0059). N.B.P.A., P.A.D., A.A.B. and C.N.H. thank the Biotechnology and Biological Sciences Research Council (BBSRC) U.K. for funding, under award numbers BB/G021546/1 and BB/M000265/1. CNH was also supported by an Advanced Award 338895 from the European Research Council.

The authors declare that they have no conflicts of interest with the contents of this article.

AUTHOR CONTRIBUTIONS

JK constructed the *Synechocystis w192a* strain and together with RS performed all *in vivo* experiments, ICV and VG performed molecular simulations and porphyrin docking. PAD prepared plasmid for expression of the recombinant W192A Gun4, NBPA and AAB designed and performed *in vitro* kinetic analyses and NBPA also determined dissociation constants. CNH contributed to the preparation of manuscript, RS and VG jointly wrote the article, RS had major responsibility for the project.

REFERENCES

1. Meskauskiene, R., Nater, M., Goslings, D., Kessler, F., den Camp, R. O., and Apel, K. (2001) FLU: A negative regulator of chlorophyll biosynthesis in *Arabidopsis thaliana*. *Proc Natl Acad Sci USA* **98**, 12826-12831
2. Apel, K., and Hirt, H. (2004) Reactive oxygen species: Metabolism, oxidative stress, and signal transduction. *Annu Rev Plant Biol* **55**, 373-399
3. Papenbrock, J., Mock, H. P., Kruse, E., and Grimm, B. (1999) Expression studies in tetrapyrrole biosynthesis: inverse maxima of magnesium chelatase and ferrochelatase activity during cyclic photoperiods. *Planta* **208**, 264-273
4. Kopečná, J., Komenda, J., Bučinská, L., and Sobotka, R. (2012) Long-term acclimation of the cyanobacterium *Synechocystis* sp PCC 6803 to high light is accompanied by an enhanced production of chlorophyll that is preferentially channeled to trimeric Photosystem I. *Plant Physiol* **160**, 2239-2250
5. Sobotka, R. (2014) Making proteins green; biosynthesis of chlorophyll-binding proteins in cyanobacteria. *Photosynth Res* **119**, 223-232

6. Czarnecki, O., and Grimm, B. (2012) Post-translational control of tetrapyrrole biosynthesis in plants, algae, and cyanobacteria. *J Exp Bot* **63**, 1675-1687
7. Sobotka, R., Komenda, J., Bumba, L., and Tichý, M. (2005) Photosystem II assembly in CP47 mutant of *Synechocystis* sp PCC 6803 is dependent on the level of chlorophyll precursors regulated by ferrochelatase. *J Biol Chem* **280**, 31595-31602
8. Sobotka, R., McLean, S., Žuberová, M., Hunter, C. N., and Tichý, M. (2008) The C-terminal extension of ferrochelatase is critical for enzyme activity and for functioning of the tetrapyrrole pathway in *Synechocystis* strain PCC 6803. *J Bacteriol* **190**, 2086-2095
9. Luo, T., Fan, T., Liu, Y., Rothbart, M., Yu, J., Zhou, S., Grimm, B., and Luo, M. (2012) Thioredoxin redox regulates ATPase activity of magnesium chelatase CHLI subunit and modulates redox-mediated signaling in tetrapyrrole biosynthesis and homeostasis of reactive oxygen species in pea plants. *Plant Physiol* **159**, 118-130
10. Gibson, L. C., Jensen, P. E., and Hunter, C. N. (1999) Magnesium chelatase from *Rhodobacter sphaeroides*: initial characterization of the enzyme using purified subunits and evidence for a BchI-BchD complex. *Biochem J* **337 (Pt 2)**, 243-251
11. Larkin, R. M., Alonso, J. M., Ecker, J. R., and Chory, J. (2003) GUN4, a regulator of chlorophyll synthesis and intracellular signaling. *Science* **299**, 902-906
12. Davison, P. A., Schubert, H. L., Reid, J. D., Iorg, C. D., Heroux, A., Hill, C. P., and Hunter, C. N. (2005) Structural and biochemical characterization of Gun4 suggests a mechanism for its role in chlorophyll biosynthesis. *Biochemistry* **44**, 7603-7612
13. Verdecia, M. A., Larkin, R. M., Ferrer, J. L., Riek, R., Chory, J., and Noel, J. P. (2005) Structure of the Mg-chelatase cofactor GUN4 reveals a novel hand-shaped fold for porphyrin binding. *PLoS Biol* **3**, e151
14. Sobotka, R., Duerhring, U., Komenda, J., Peter, E., Gardian, Z., Tichý, M., Grimm, B., and Wilde, A. (2008) Importance of the cyanobacterial GUN4 protein for chlorophyll metabolism and assembly of photosynthetic complexes. *J Biol Chem* **283**, 25794-25802
15. Formighieri, C., Ceol, M., Bonente, G., Rochaix, J. D., and Bassi, R. (2012) Retrograde signaling and photoprotection in a gun4 mutant of *Chlamydomonas reinhardtii*. *Mol Plant* **5**, 1242-1262
16. Adhikari, N. D., Orler, R., Chory, J., Froehlich, J. E., and Larkin, R. M. (2009) Porphyrins promote the association of GENOMES UNCOUPLED 4 and a Mg-chelatase subunit with chloroplast membranes. *J Biol Chem* **284**, 24783-24796
17. Adams, N. B. P., Marklew, C. J., Qian, P., Brindley, A. A., Davison, P. A., Bullough, P. A., and Hunter, C. N. (2014) Structural and functional consequences of removing the N-terminal domain from the magnesium chelatase ChIH subunit of *Thermosynechococcus elongatus*. *Biochem J* **464**, 315-322
18. Karger, G. A., Reid, J. D., and Hunter, C. N. (2001) Characterization of the binding of deuteroporphyrin IX to the magnesium chelatase H subunit and spectroscopic properties of the complex. *Biochemistry* **40**, 9291-9299
19. Peter, E., and Grimm, B. (2009) GUN4 is required for posttranslational control of plant tetrapyrrole biosynthesis. *Mol Plant* **2**, 1198-1210
20. Brzezowski, P., Schlicke, H., Richter, A., Dent, R. M., Niyogi, K. K., and Grimm, B. (2014) The GUN4 protein plays a regulatory role in tetrapyrrole biosynthesis and chloroplast-to-nucleus signalling in *Chlamydomonas reinhardtii*. *Plant J* **79**, 285-298
21. Adhikari, N. D., Froehlich, J. E., Strand, D. D., Buck, S. M., Kramer, D. M., and Larkin, R. M. (2011) GUN4-Porphyrin Complexes Bind the ChlH/GUN5 Subunit of Mg-Chelatase and Promote Chlorophyll Biosynthesis in *Arabidopsis*. *Plant Cell* **23**, 1449-1467

22. Case, D. A., Darden, T. E., Cheatham, I., T. E., Simmerling, C. L., Wang, J., Duke, R. E., Luo, R., Walker, R. C., Zhang, W., Merz, K. M., Roberts, B., Wang, B., Hayik, S., Roitberg, A., Seabra, G., LKolossváry, I., Wong, K. F., Paesani, F., Vanicek, J., Liu, J., Wu, X., Brozell, S. R., Steinbrecher, T., Gohlke, H., Cai, Q., Ye, X., Wang, J., Hsieh, M.-J., Cui, G., Roe, D. R., Mathews, D. H., Seetin, M. G., Sagui, C., Babin, V., Luchko, T., Gusarov, S., Kovalenko, A., and Kollman, P. A. (2010) Amber 11. University of California, San Francisco
23. Sastry, G. M., Adzhigirey, M., Day, T., Annabhimoju, R., and Sherman, W. (2013) Protein and ligand preparation: parameters, protocols, and influence on virtual screening enrichments. *J Comput Aided Mol Des* **27**, 221-234
24. Borrelli, K. W., Vitalis, A., Alcantara, R., and Guallar, V. (2005) PELE: Protein energy landscape exploration. A novel Monte Carlo based technique. *Journal of Chemical Theory and Computation* **1**, 1304-1311
25. Lee, J., Lee, H. J., Shin, M. K., and Ryu, W. S. (2004) Versatile PCR-mediated insertion or deletion mutagenesis. *BioTechniques* **36**, 398-400
26. Porra, R. J., Thompson, W. A., and Kriedemann, P. E. (1989) Determination of accurate extinction coefficients and simultaneous equations for assaying chlorophylls *a* and *b* extracted with four different solvents: verification of the concentration of chlorophyll standards by atomic absorption spectroscopy. *Biochim Biophys Acta* **975**, 384-394
27. Pilný, J., Kopečná, J., Noda, J., and Sobotka, R. (2015) Detection and quantification of heme and chlorophyll precursors using a High Performance Liquid Chromatography (HPLC) system equipped with two fluorescence detectors. *Bio-protocol* **5**, e1390
28. Adams, N. B., Marklew, C. J., Brindley, A. A., Hunter, C. N., and Reid, J. D. (2014) Characterization of the magnesium chelatase from *Thermosynechococcus elongatus*. *Biochem J* **457**, 163-170
29. Jensen, P. E., Gibson, L. C. D., Henningsen, K. W., and Hunter, C. N. (1996) Expression of the chlI, chlD, and chlH genes from the cyanobacterium *Synechocystis* PCC6803 in *Escherichia coli* and demonstration that the three cognate proteins are required for magnesium-protoporphyrin chelatase activity. *J Biol Chem* **271**, 16662-16667
30. Kotev, M., Lecina, D., Tarrago, T., Giralt, E., and Guallar, V. (2015) Unveiling prolyl oligopeptidase ligand migration by comprehensive computational techniques. *Biophys J* **108**, 116-125
31. Madadkar-Sobhani, A., and Guallar, V. (2013) PELE web server: atomistic study of biomolecular systems at your fingertips. *Nucleic Acids Res* **41**, W322-328
32. Hernandez-Ortega, A., Borrelli, K., Ferreira, P., Medina, M., Martinez, A. T., and Guallar, V. (2011) Substrate diffusion and oxidation in GMC oxidoreductases: an experimental and computational study on fungal aryl-alcohol oxidase. *Biochem J* **436**, 341-350
33. Chen, X., Pu, H., Wang, X., Long, W., Lin, R., and Liu, L. (2015) Crystal Structures of GUN4 in Complex with Porphyrins. *Mol Plant* **8**, 1125-1127
34. Tarahi Tabrizi, S., Langley, D. B., Harrop, S. J., Duff, A. P., and Willows, R. D. (2015) Structure of GUN4 from Chlamydomonas reinhardtii. *Acta Crystallogr F Struct Biol Commun* **71**, 1094-1099
35. Guallar, V., Jacobson, M., McDermott, A., and Friesner, R. A. (2004) Computational modeling of the catalytic reaction in triosephosphate isomerase. *J Mol Biol* **337**, 227-239
36. Kopečná, J., Pilný, J., Krynická, V., Tomčala, A., Kis, M., Gombos, Z., Komenda, J., and Sobotka, R. (2015) Lack of phosphatidylglycerol inhibits chlorophyll biosynthesis at

multiple sites and limits chlorophyllide reutilization in the cyanobacterium *Synechocystis* 6803. *Plant Physiol*

37. Susek, R. E., Ausubel, F. M., and Chory, J. (1993) Signal transduction mutants of *Arabidopsis* uncouple nuclear CAB and RBCS gene expression from chloroplast development. *Cell* **74**, 787-799
38. Grovenstein, P. B., Wilson, D. A., Lankford, K. D., Gaston, K. A., Perera, S., and Mitra, M. (2013) Identification and molecular characterization of the second Chlamydomonas gun4 mutant, gun4-II. *F1000Res* **2**, 142
39. Mochizuki, N., Tanaka, R., Tanaka, A., Masuda, T., and Nagatani, A. (2008) The steady-state level of Mg-protoporphyrin IX is not a determinant of plastid-to-nucleus signaling in Arabidopsis. *Proc Natl Acad Sci U S A* **105**, 15184-15189
40. Papenbrock, J., Mock, H. P., Tanaka, R., Kruse, E., and Grimm, B. (2000) Role of magnesium chelatase activity in the early steps of the tetrapyrrole biosynthetic pathway. *Plant Physiol* **122**, 1161-1169
41. Papenbrock, J., Mishra, S., Mock, H. P., Kruse, E., Schmidt, E. K., Petersmann, A., Braun, H. P., and Grimm, B. (2001) Impaired expression of the plastidic ferrochelatase by antisense RNA synthesis leads to a necrotic phenotype of transformed tobacco plants. *Plant J* **28**, 41-50
42. Shepherd, M., McLean, S., and Hunter, C. N. (2005) Kinetic basis for linking the first two enzymes of chlorophyll biosynthesis. *FEBS J* **272**, 4532-4539
43. Papenbrock, J., Pfundel, E., Mock, H. P., and Grimm, B. (2000) Decreased and increased expression of the subunit CHL I diminishes Mg chelatase activity and reduces chlorophyll synthesis in transgenic tobacco plants. *Plant J* **22**, 155-164

FIGURE LEGENDS

Figure 1. **An overview of original Gun4 structures and the prediction of** α2/α3 and α6/α7 **loops**. **A**) Comparison of two cyanobacterial Gun4 crystal structures; *T.el* (in blue) and *Syn* (in gold) corresponding to the PDB codes 1Z3X and 1Y6I, respectively (12,13). Loops involved in opening of the binding site (see main text) are highlighted. Ovals indicate sites of crystal contacts in the symmetric units. The inset shows position of Leu105 (*T.el*) buried among α1, α2 and α4 helixes. **B**) Alignment of the original *T.el* structure (in beige) and the *Syn* (in gold) and *T.el* (in blue) structures after loop predictions by Prime. Note the similar orientation of Trp192 and Tyr197 residues. **C**) The original loop orientation and the position of Trp192 residue in the *Syn* Gun4 structure (green color) compared with the lowest energy predictions by Prime without crystal mates (in red). The α2/α3 loop corresponds to Pro122-Phe132 residues and the highlighted part of the α6/α7 loop corresponds to Ser185-Gly195.

Figure 2. **Four snapshots along the porphyrin migration pathway and binding site entrance in *Syn* Gun4**. **A**) Initial structure with a bulk solvent exposed ligand. **B**) Pre-docking pose with stacking onto Arg113 and hydrogen bonds with Gln126 and Gln128 in the α2/α3 loop. **C**) Pocket-A bound structure with an iron axial coordination-like motif with Asn211 and Arg113. **D**) Pocket-B bound deeper structure.

Figure 3. **Interaction between MgP and Gun4 residues in two putative binding pockets identified by the PELE simulation**. Diagrams (**A**) and (**B**) correspond to the position of MgP depicted in Fig. 2C and Fig. 2D, respectively. Line discontinuities in the vicinity of the propionate groups indicate larger exposure to solvent. Arrows represent hydrogen bonds, dashed line in (A) highlights co-ordination of MgP by Asn211 residue and red arrowhead shows Trp192 residue selected for mutagenesis. Residues marked by asterisk were analyzed by site-directed mutagenesis in previous reports (12,13) and in this report for Trp192; green asterisks indicate minimal effect of the replacement of given residue on porphyrin binding (an increase of $K_d < 2$ for MgP or P_{IX}), blue means a moderate effect (2-5), red asterisks mark residues, which mutation increased K_d more than five-times. Gray dots mark residues for which no data are available.

Figure 4. Analyses of the protein-MgP interaction energies by PELE. A) Protein-ligand interaction energy against the distance to Asn211 (side chain oxygen atom) along the refinement process for the *Syn* Gun4. **B**) The result of a 4 kcal/mol binning of the interaction energies for the Gun4 (red) and the W192A (green) mutant protein.

Figure 5. Circular-dichroism spectra of the recombinant *Syn* Gun4 protein and its mutated W192A variant.

Figure 6. A representative snapshot for the refinement of MgP docking in the *Syn* Gun4 protein. The direct Van der Waals interaction between Trp192 and the porphyrin ligand is indicated.

Figure 7. **Molecular dynamics analysis of the *T.el* WT Gun4 and L105F mutant**. **A**) RMSF for both species. **B**) Cross-correlation differences between *T.el* WT and the L105F mutant. The black circles highlight the region corresponding to helix 2 and the α6/α7 loop.

Figure 8. ***In vitro*** **stimulation of the MgCh activity by *Syn* Gun4 and W192A proteins**. Assembly titrations of MgCh and WT Gun4 (circles) or W192A (squares). Assays contained 0.1 μM ChlD, 0.2 μM ChlI and 0.4 μM ChlH in 50 mM MOPS/KOH, 0.3 M glycerol, 1 mM DTT, 1 mM free Mg^{2+}, I = 0.1 with KCl, pH 7.7 at 34 °C and closed symbols 8 μM D_{IX}, open symbols 0.8 μM D_{IX}. The curves at 8 μM D_{IX} can be described by equation 1, and at 0.8 μM D_{IX} with equation 2, with characterizing parameters in table II.

Figure 9. **Chl biosynthesis in the *Syn gun4-W192* strain**. **A**) Whole cell absorbance spectra of the *Syn* WT and *gun4-W192A* strain (W192A) grown at 30 and 300 μmol of photons m^{-2} s^{-1}. Chl is represented by 680 nm peak and phycobilinoproteins by the 625 nm peak. Spectra were normalized to light scattering at 750 nm. The total Chl content per optical density is indicated. **B**) Immunodetection of Gun4, MgCh ChlH and ChlI subunits, ChlM and ferrochelatase (FeCH) in the WT and *gun4-W192A* strains grown under saturating light and during nitrogen depletion and re-greening (see Results and Fig. 10 for details). The membrane (m) and soluble (s) protein fractions were separated by SDS-electrophoresis, blotted, and probed using indicated antibodies. Purple asterisk marks an unspecific cross-reaction or, potentially, a low-abundant variant of ChlH. **C**) The relative levels of Chl precursors in the *gun4-W192A* strain in comparison to the WT. Values shown represent means ± SD from five independent measurements. Asterisks indicate statistically significant differences in precursor levels as tested using a paired Student's t-test (*, P = 0.05; **, P = 0.01). CoPP, coproporphyrin(ogen) III; P_{IX}, protoporphyrin(ogen) IX; MgPME, MgP methyl ester; DV-PChlide, divinyl-protochlorophyllide; MV-PChlide, monovinyl-protochlorophyllide; DV-Chlide, divinyl-chlorophyllide; MV-Chlide, monovinyl-chlorophyllide.

Figure 10. **Analysis of Chl precursors in the *Syn* WT and *gun4-W192* strains during recovery from nitrogen starvation. A)** Levels of Chl precursors in cells grown under saturating light without nitrogen for 16 hours and (**B**) 2 hours after adding of 10 mM $NaNO_3$. Extracted pigments were analyzed by HPLC equipped with a pair of fluorescence detectors (FLD1 and FLD2) set for different wavelengths to cover all Chl precursors from coproporphyrinogen III (oxidized spontaneously to coproporphyrin III) to monovinyl-chlorophyllide. Pigments are labelled as in Fig. 9.

TABLES

Table I. Dissociation constants (K_d) for the *Syn* Gun4 protein and W192A mutant. Dissociation constants were calculated for deuteroporphyrin IX (D_{IX}) and Mg-deuteroporphyrin IX (MgD), monitoring tryptophan fluorescence quenching (see Experimental procedures for details).

protein	D_{IX} K_d (μM)	MgD K_d (μM)
Syn Gun4	3.83 ± 0.39	2.5 ± 0.09
Syn W192A	7.32 ± 0.61	7.22 ± 0.82

Table II. Apparent binding constants of *Syn* WT and W192A-Gun4 to the core MgCh complex. * Fitted to equation 1. † Fitted to equation 2 (see Experimental procedures for details).

protein	D_{IX} conc. (μM)	V_{max} (μM min^{-1})	K_{app} (μM)	K_{iapp} (μM)
Gun4	8*	0.444 ± 0.14	0.094 ± 0.059	0.540 ± 0.356
	0.8†	0.061 ± 0.005	0.043 ± 0.013	--
W192A	8*	0.529 ± 0.168	0.261 ± 0.133	0.523 ± 0.295
	0.8†	0.0328 ± 0.003	0.164 ± 0.063	--

FIGURES

Figure 1

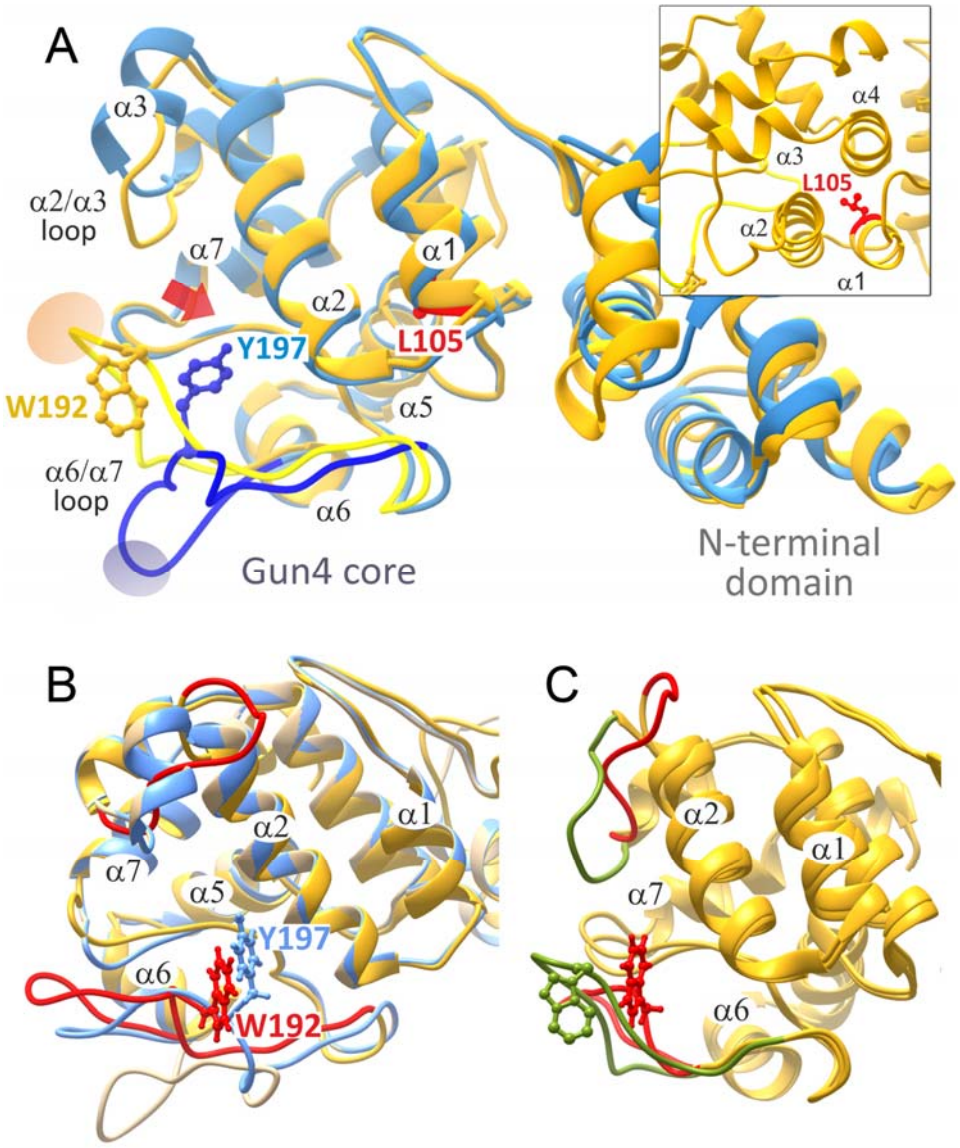

Figure 2

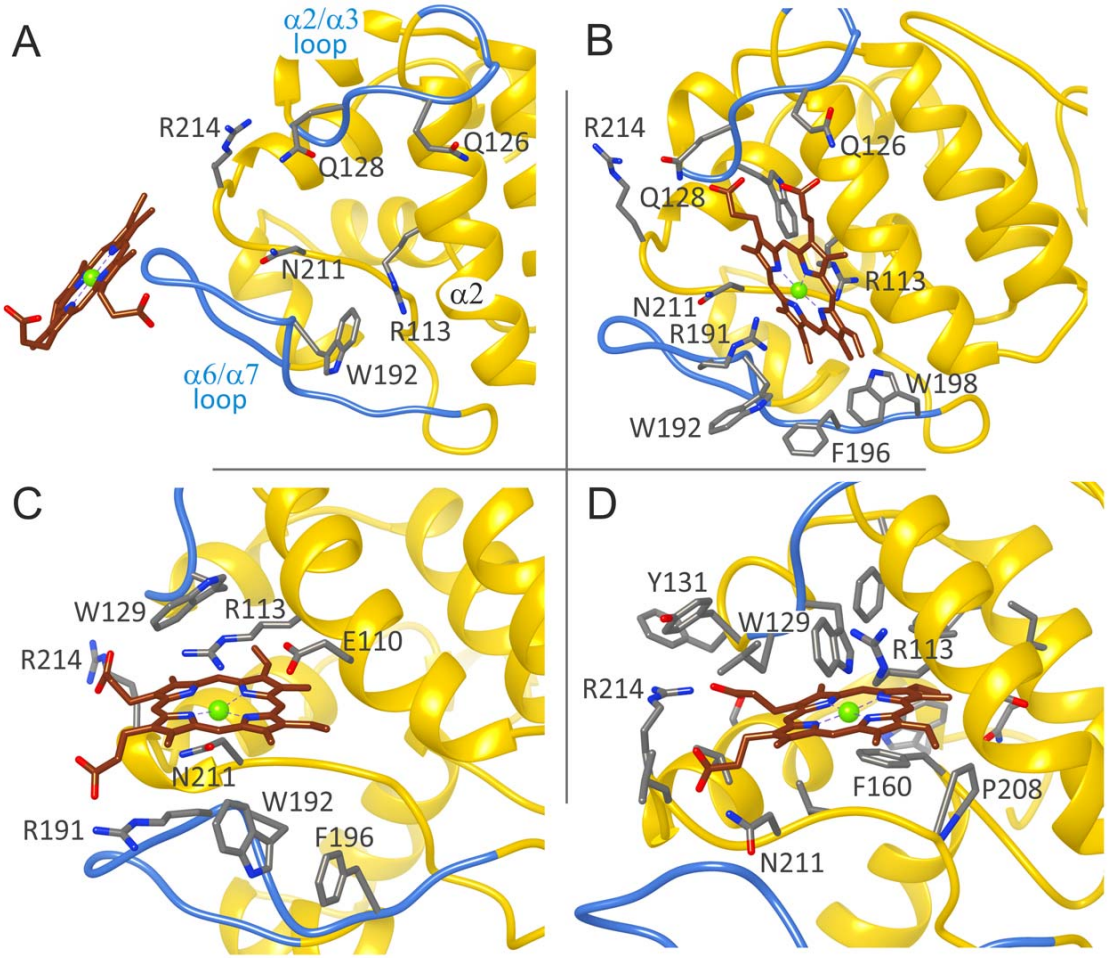
A
α2/α3 loop
R214
Q126
Q128
N211
α2
R113
α6/α7 loop
W192
B
R214
Q126
Q128
R113
N211
R191
W198
W192
F196
C
W129
R113
E110
R214
N211
W192
R191
F196
D
Y131
W129
R113
R214
F160
P208
N211

Figure 3

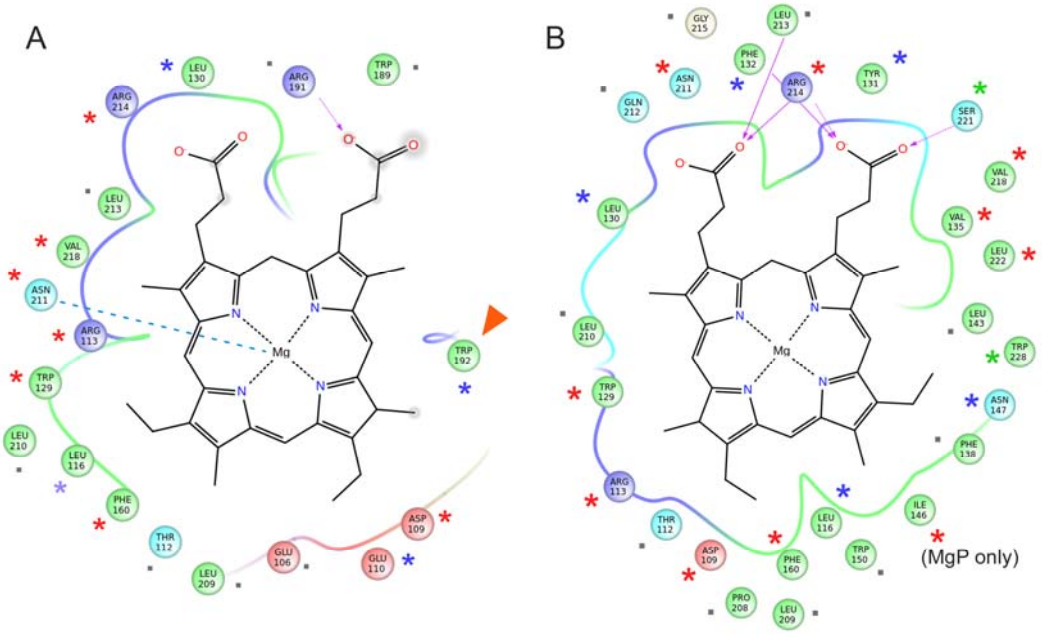

Figure 4

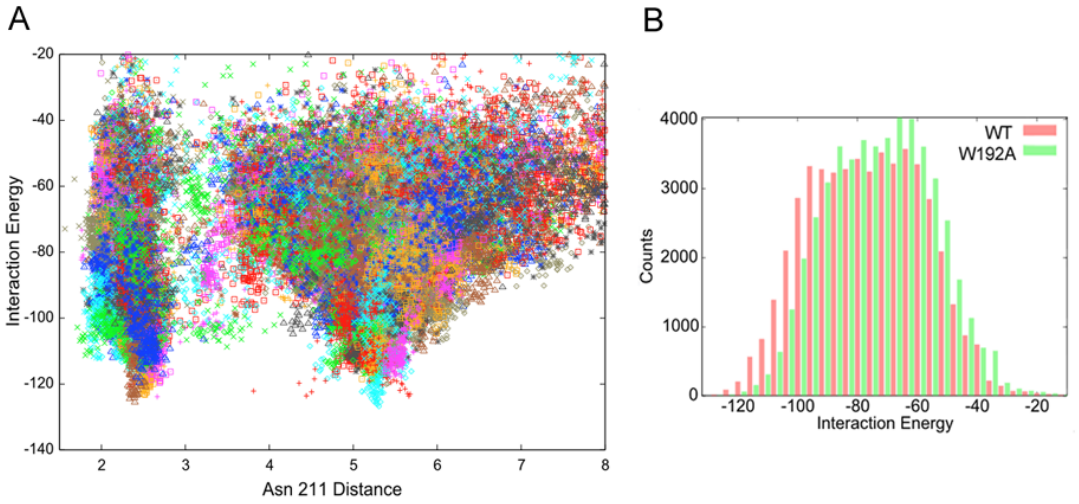

Figure 5

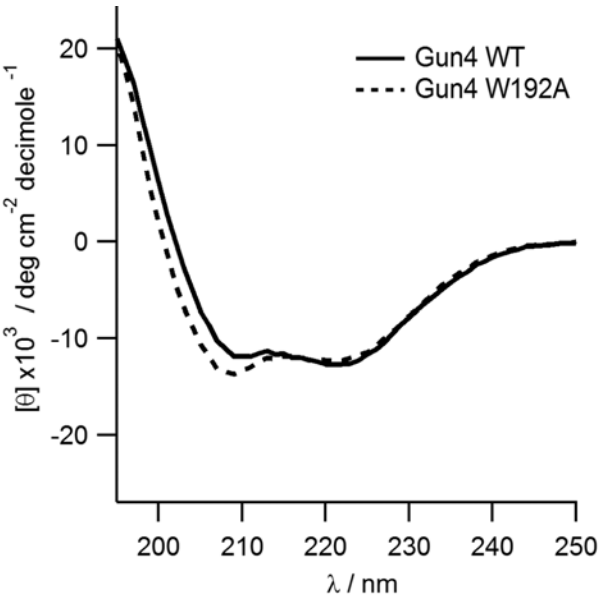

Figure 6

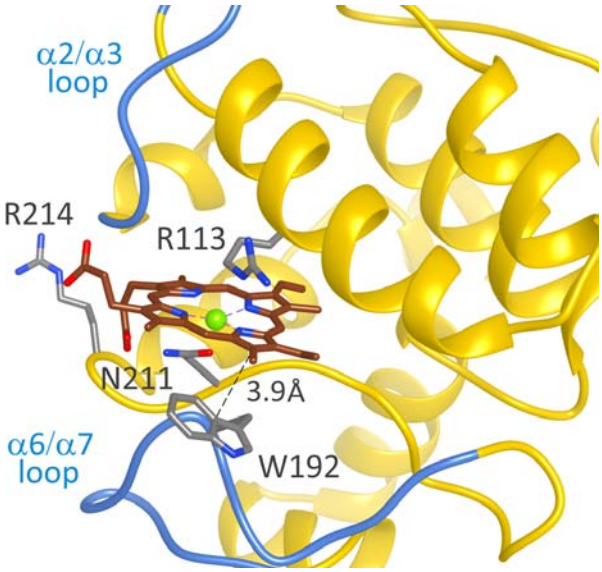

Figure 7

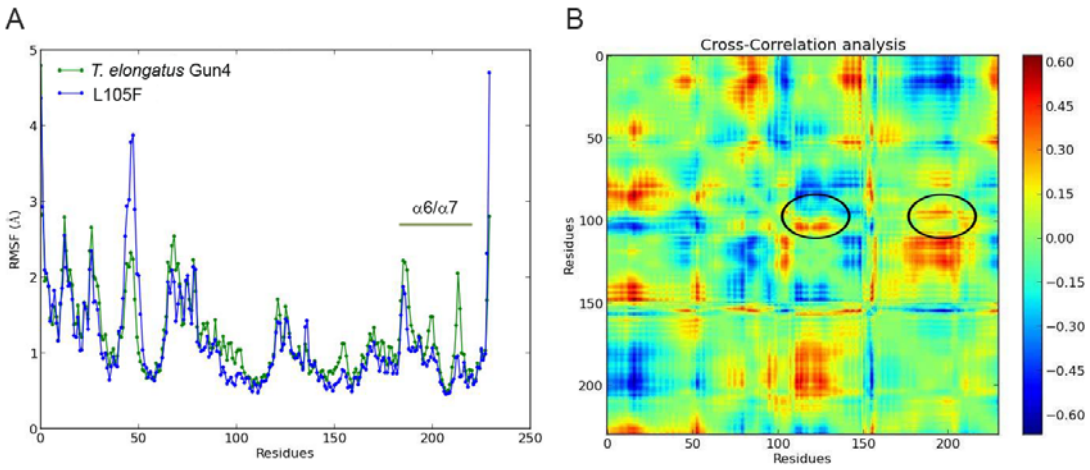

Figure 8

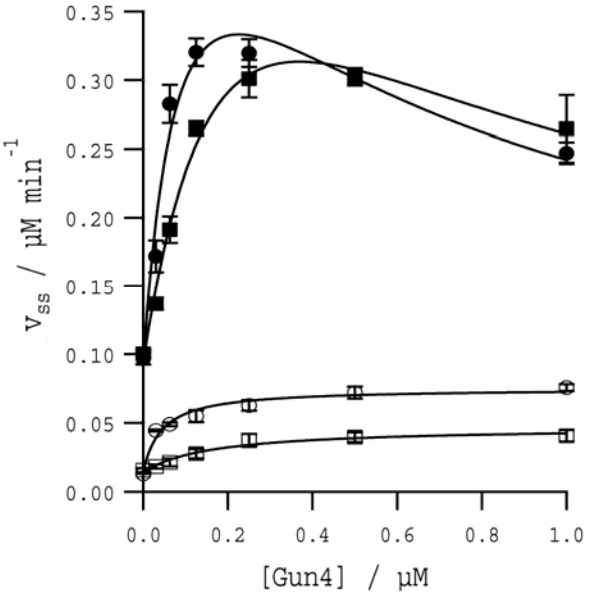

.

Figure 9

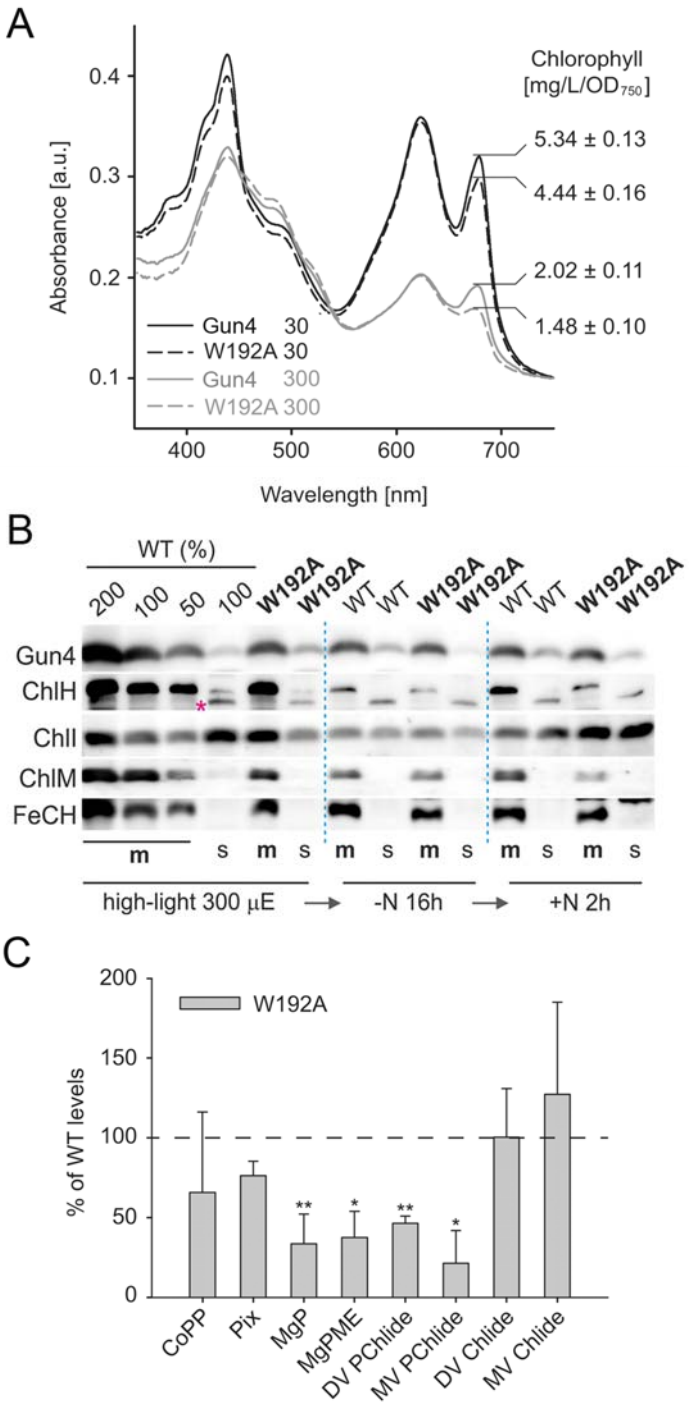
A
Chlorophyll
[mg/L/OD750]
5.34 ± 0.13
4.44 ± 0.16
2.02 ± 0.11
1.48 ± 0.10
Absorbance [a.u.]
Gun4 30
W192A 30
Gun4 300
W192A 300
Wavelength [nm]
B
WT (%)
200 100 50 100 W192A W192A WT WT W192A W192A WT WT W192A W192A
Gun4
ChlH
ChlI
ChlM
FeCH
m s m s m s m s m s m s
high-light 300 µE
-N 16h
+N 2h
C
W192A
% of WT levels
CoPP Pix MgP MgPME DV PChlide MV PChlide DV Chlide MV Chlide

Figure 10

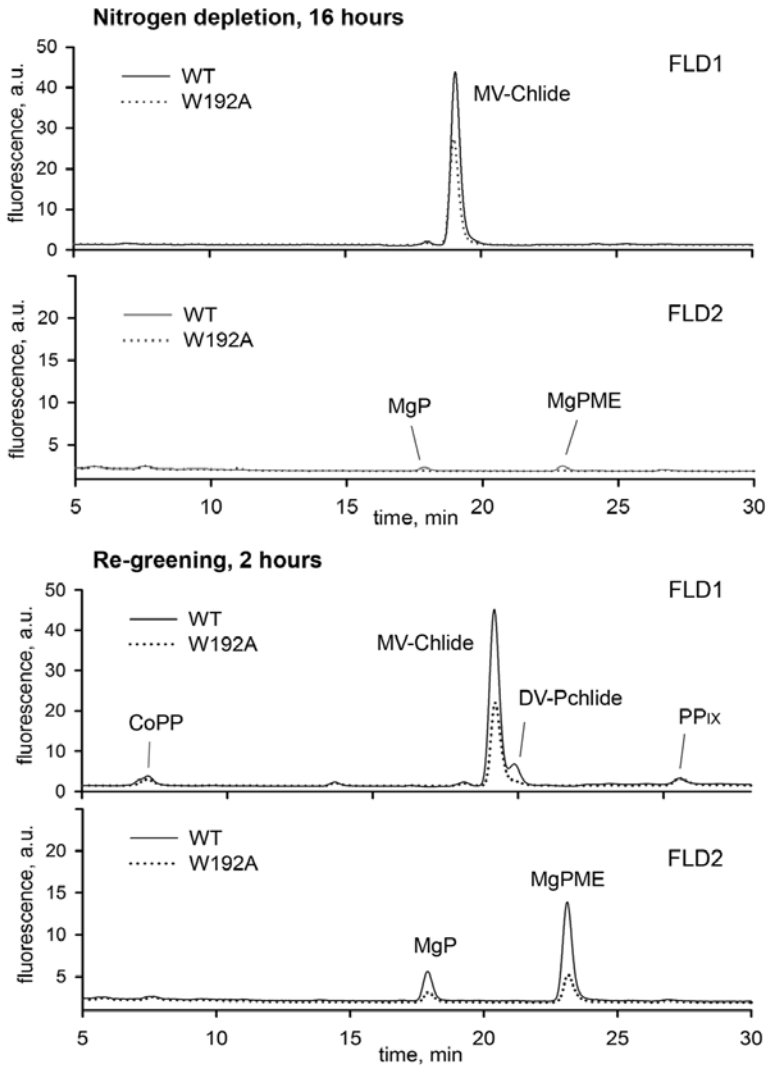
Nitrogen depletion, 16 hours
FLD1
WT
W192A
MV-Chlide
fluorescence, a.u.
FLD2
MgP
MgPME
time, min
Re-greening, 2 hours
CoPP
DV-Pchlide
PPIX